Bayesian Compressive Sensing-based Method for Directions-of-Arrival Estimation

M.Carlin, P. Rocca, G. Oliveri, and A. Massa

Abstract

In this report, the estimation of the directions of arrival (DoAs) of narrow-band signals impinging on a linear antenna array is addressed within the Bayesian compressive sensing (BCS) framework. Unlike several state-of-the-art approaches, the voltages at the output of the receiving sensors are directly used to determine the DoAs of the signals thus avoiding the computation of the correlation matrix. Towards this end, the estimation problem is properly formulated to enforce the sparsity of the solution in the linear relationships between output voltages (i.e., the problem data) and the unknown DoAs. A careful calibration of the BCS parameters is reported in the report after the problem formulation.

Contents

1 Mathematical Formulation

1.1 Measurement model

Let us consider an array composed by a set of M antennas located at positions

$$\mathbf{r} \quad = \quad x_m \hat{\mathbf{x}} = (m-1)\, d \tag{1}$$

with $m = 1, \ldots, M$, where d is the distance among the receiving elements (expressed in multiple of λ), which are supposed to be equally spaced. The M antennas receive the electromagnetic waves generated by L far field sources.

The electromagnetic field at each receiving antenna is a linear combination of the incident electromagnetic waves, i.e.,

$$\mathbf{E}^{inc}(\mathbf{r}) \quad = \quad \sum_{L=1}^{L} \mathbf{E}_l^{inc}(\mathbf{r}) \tag{2}$$

where $\mathbf{E}_l^{inc}(\mathbf{r})$, $l = 1, \ldots, L$ denotes the electromagnetic field of the lth incoming wave.

In this work, this field is supposed to be $\hat{\mathbf{y}}$-polarized and the propagation limited to the $x - z$ plane. Since the electromagnetic sources are located in the far-field region of the array, the received electromagnetic waves are plane waves, i.e.

$$\mathbf{E}_l^{inc}(\mathbf{r}) \quad = \quad E_l^{inc}(x, z)\, \hat{\mathbf{y}} = E_l^{inc} e^{j2\pi x_m sin(\theta_l)/\lambda} \hat{\mathbf{y}} \tag{3}$$

where θ_l, $l = 1, \ldots, L$, is the DOA of the mth wave $(\phi_l = 0,\, l = 1, \ldots, L)$, $E_l^{inc} \in \mathbb{R}$, $l = 1, \ldots, L$, is the **real** amplitude of the lth plane wave and λ is the signal wavelength.

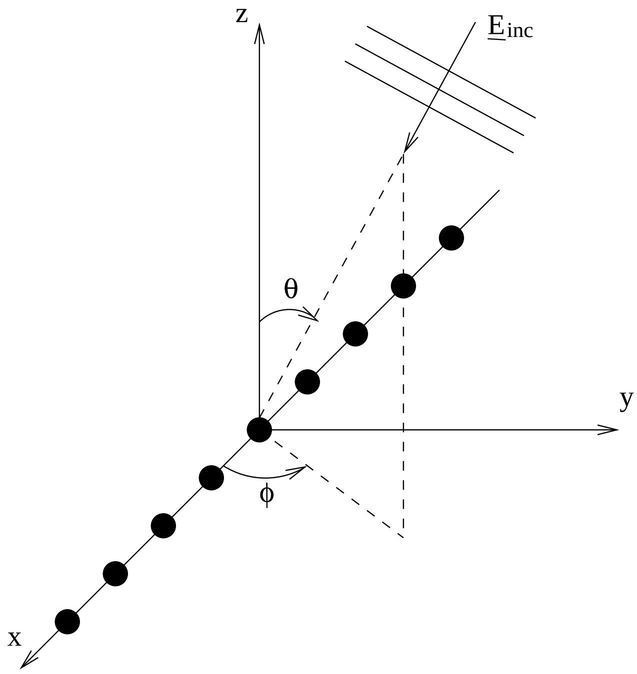

Figure 1: Reference geometry.

Moreover, the angular separation between two adjacent waves is denoted by $\Delta\theta^{l(l+1)}$, and it is defined as

$$\Delta\theta^{l(l+1)} = \theta_{l+1} - \theta_l, \; l = 1, \dots, L. \tag{4}$$

The open-circuit output voltage of the mth antenna is given by

$$\nu_m = \mathbf{E}^{inc}(\mathbf{r}_m) \cdot \mathbf{l}_e^m + n_m = \sum_{l=1}^{L} \mathbf{E}_l^{inc}(\mathbf{r}_m) \cdot \mathbf{l}_e^m + n_m \tag{5}$$

where $\mathbf{l}_e^m$ is the effective length of the mth element, and n_m, $m = 1, \dots, M$, is a Gaussian Noise (assumed with zero mean value and variance σ^2).

By substituting (2) in (5) and considering an uniform array with elements characterized by effective length $\mathbf{l}_e^1 = \mathbf{l}_e^2 = \dots = \mathbf{l}_e^M = \mathbf{l} = \hat{\mathbf{x}} + \hat{\mathbf{y}} + \hat{\mathbf{z}}$ (isotropic antennas), the the open-circuit voltage at the output of the mth antenna results to be given by

$$\nu_m = \sum_{l=1}^{L} E_l^{inc} e^{j2\pi x_m sin(\theta_l)/\lambda} \hat{\mathbf{y}} \cdot \mathbf{l} + n_m = \sum_{l=1}^{L} E_l^{inc} e^{j2\pi x_m sin(\theta_l)/\lambda} + n_m. \tag{6}$$

By using the matrix notation, the voltages (6) can be rewritten as

$$\underline{\nu}(t_s) = \mathbf{A}(\underline{\theta})\,\underline{x} + \underline{n}, \tag{7}$$

where

- $\underline{\theta} = [\theta_1, ..., \theta_L]$ is the DOA of the l-th signal.
- $\underline{\nu} = [\nu_1, ..., \nu_M]^T$is the vector of measured data and $\nu_m \in \mathbb{C}$ is the open circuit voltage measured at the mth array element.
- $\mathbf{A}(\underline{\theta}) = [\underline{a}(\theta_1), .., \underline{a}(\theta_L)]$ is the steering matrix and

$$\underline{a}(\theta_l) = \begin{bmatrix} e^{j2\pi x_m sin(\theta_l)/\lambda} & \dots & e^{j2\pi x_m sin(\theta_l)/\lambda} & \dots & e^{j2\pi x_m sin(\theta_l)/\lambda} \end{bmatrix}^T \quad (8)$$

  is the steering vector for the lth signal.
- x_m is the location of the mth array element $(m = 1, \dots, M)$.
- $\underline{n} = [n_1, ..., n_M]^T$ is a vector of $AWGN$ complex noise samples and $n_m \in \mathbb{C}$ is the complex noise affecting the mth receiver.
- $\underline{x} = \left[E_1^{inc}, ..., E_L^{inc}\right]^T$ with $E_l^{inc} \in \mathbb{R}$ is the vector of impinging waves amplitudes at the receivers locations.

1.2 BCS DOA estimation

Hypothesis: DOAs θ_l, $l = 1, \dots, L$, of the incident signals belonging to a user-chosen set of $K \gg M > L$ angular positions $\underline{\hat{\theta}} = \left[\hat{\theta}_1, ..., \hat{\theta}_K\right]$, $\hat{\theta}_k = -\frac{\pi}{2} + \frac{(k-1)\cdot\pi}{K-1}$, $k = 1, \dots, K$.

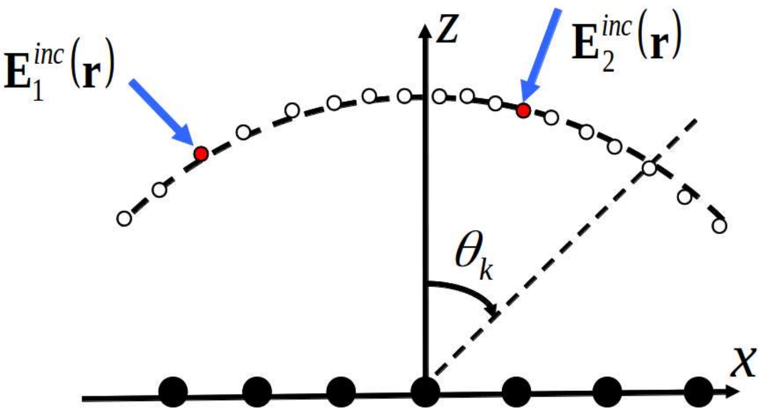

Figure 2: Fine sampling of the angular range of interest.

Let us define the sparse DOA vector $\underline{\hat{x}} = [\hat{x}_1, ..., \hat{x}_K]^T$ encoding both θ_l and E_l^{inc}

$$\hat{x}_k = \begin{cases} E_l^{inc} & if\, \hat{\theta}_k = \theta_l \\ 0 & otherwise \end{cases} . \quad (9)$$

Then we define a new matrix of steering vectors (which is known)

$$\mathbf{A}\left(\underline{\hat{\theta}}\right) \triangleq \begin{bmatrix} \exp\left(\frac{j2\pi x_1 sin\left(\hat{\theta}_1\right)}{\lambda}\right) & \cdots & \exp\left(\frac{j2\pi x_1 sin\left(\hat{\theta}_K\right)}{\lambda}\right) \\ \vdots & \ddots & \vdots \\ \exp\left(\frac{j2\pi x_m sin\left(\hat{\theta}_1\right)}{\lambda}\right) & \cdots & \exp\left(\frac{j2\pi x_m sin\left(\hat{\theta}_K\right)}{\lambda}\right) \end{bmatrix} \tag{10}$$

The objective is to use BCS solver to find the most probable sparse vector $\underline{\hat{x}}$ satisfying the equation

$$\underline{\nu} = \mathbf{A}\left(\underline{\hat{\theta}}\right)\underline{\hat{x}} + \underline{n}. \tag{11}$$

Since the BCS approach addresses only purely real valued problems and (11) includes complex-valued vectors and matrices, the equation (11) is rewritten as

$$\begin{bmatrix} \Re\{\underline{\nu}\} \\ \Im\{\underline{\nu}\} \end{bmatrix} = \begin{bmatrix} \Re\left\{\mathbf{A}\left(\underline{\hat{\theta}}\right)\right\} & -\Im\left\{\mathbf{A}\left(\underline{\hat{\theta}}\right)\right\} \\ \Im\left\{\mathbf{A}\left(\underline{\hat{\theta}}\right)\right\} & \Re\left\{\mathbf{A}\left(\underline{\hat{\theta}}\right)\right\} \end{bmatrix} \begin{bmatrix} \Re\{\underline{\hat{x}}\} \\ \Im\{\underline{\hat{x}}\} \end{bmatrix} + \begin{bmatrix} \Re\{\underline{n}\} \\ \Im\{\underline{n}\} \end{bmatrix}, \tag{12}$$

where $\Re\{\cdot\}$ and $\Im\{\cdot\}$ identify the real and imaginary parts.

1.3 Noise definition

The noise sequence $\underline{n}$ includes background and electronic noise and is characterized by the following properties

- Gaussian distribution
- Zero mean
- Temporally and spatially white
- Uncorrelated with the emitter signals
- Variance (power) σ_n^2
- Complex $\Rightarrow$ $n_m = \Re\{n_m\} + j\Im\{n_m\}$

Where $\Re\{n_m\}$ and $\Im\{n_m\}$ are real samples of $AWGN$ noise with variance $\sigma_n^2/2$.

1.4 BCS parameters

One of input parameters of the BCS solver is the estimation of the noise variance σ^2 which is computed as

$$\sigma^2 = \mathrm{std}\left(\underline{\nu}\right)^2 \sigma_0^2 \quad , \tag{13}$$

where $\mathrm{std}(\underline{\nu})$ is the standard deviation of the measured voltages. Since $\underline{\nu}$ is a complex vector, its standard deviation is defined as (from MATLAB help)

$$\mathrm{std}(\underline{\nu}) = \sqrt{\mathrm{std}\{\Re[\underline{\nu}]\}^2 + \mathrm{std}\{\Im[\underline{\nu}]\}^2} \quad , \tag{14}$$

where

$$\begin{aligned} \mathrm{std}\{\Re[\underline{\nu}]\} &= \sqrt{\frac{1}{M-1}\sum_{m=1}^{M}\left[\Re(\nu_m) - \nu_{\Re}^{(ave)}\right]^2} \\ \mathrm{std}\{\Im[\underline{\nu}]\} &= \sqrt{\frac{1}{M-1}\sum_{m=1}^{M}\left[\Im(\nu_m) - \nu_{\Im}^{(ave)}\right]^2} \end{aligned} \tag{15}$$

with $\nu_{\Re}^{(ave)} = \sum_{m=1}^{M}\Re(\nu_m)$ and $\nu_{\Im}^{(ave)} = \sum_{m=1}^{M}\Im(\nu_m)$.

1.5 Number of signals L estimation

Starting from the estimated vector $\underline{\hat{x}} = [\hat{x}_1, ..., \hat{x}_K]^T$, the number of impinging signals L can be estimated by simply counting the non-zero elements of $\underline{\hat{x}}$. The problem is that there are non-zero elements of $\underline{\hat{x}}$ that does not correspond to any actual signal and are produced by the presence of the noise. Then, in order to improve the reliability of the achieved element count, the idea it to remove the lowest-energy components of $\underline{\hat{x}}$ by applying the following procedure.

1. First we remove all the lowest-energy elements of the vector $\underline{\hat{x}}$, stopping before the condition $\sum_{k=1}^{K}\xi_k \geq \eta$ (where $0 \leq \eta \leq 1.0$ is a user-defined energy threshold) is no longer satisfied, where ξ_k is defined as $\xi_k = \frac{|\hat{x}_k|^2}{\sum_{k=1}^{K}|\hat{x}_k|^2}$.

2. Then the estimated number of impinging signals $\widetilde{L}$ can be obtained by counting the number of remaining elements in $\underline{\hat{x}}$. In other words

$$\widetilde{L} = \sum_{k=1}^{K} H(|\hat{x}_k|),$$

where $H(\cdot)$ is the unit step function, defined as $H(\hat{x}_k) = \begin{cases} 0 & if\ \hat{x}_k \leq 0 \\ 1 & otherwise \end{cases}$.

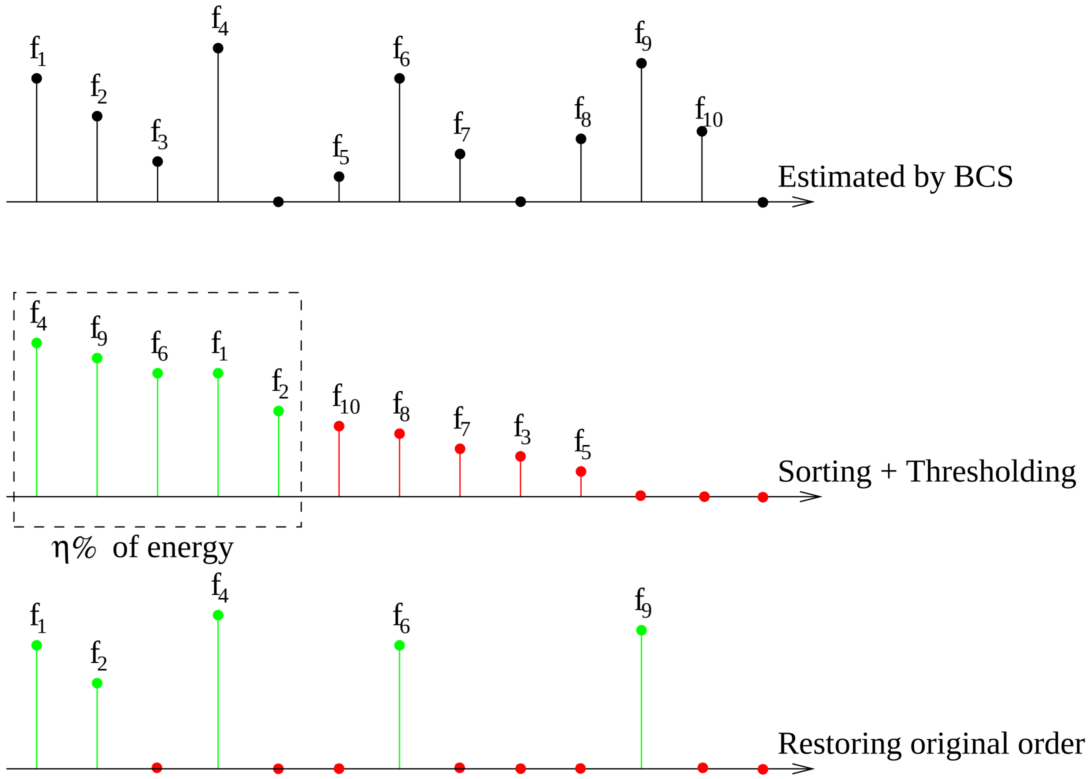

Figure 3: Thresholding operation.

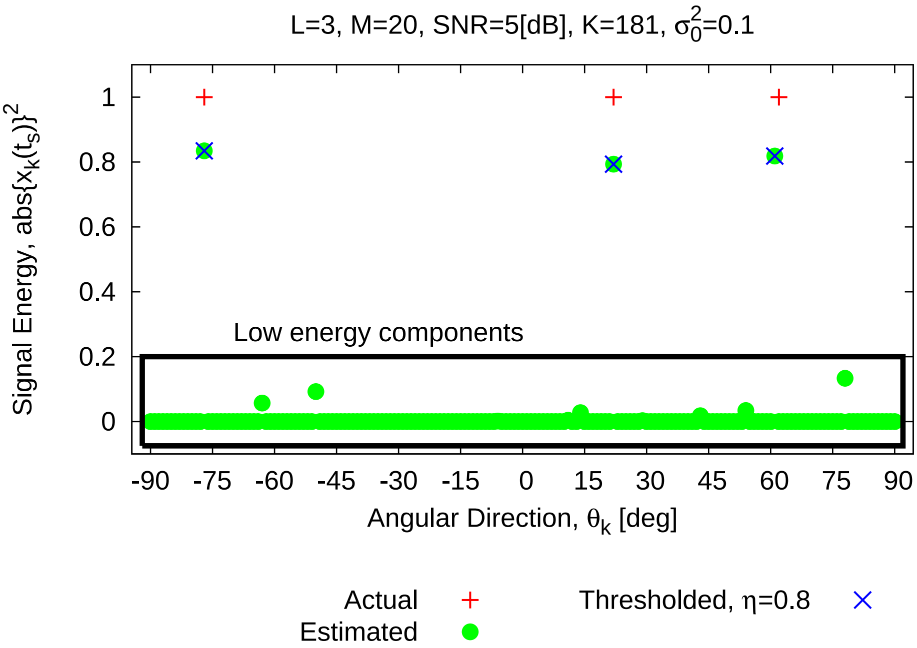

Figure 4: *BCS DoA estimation* - actual vector $\underline{f}(t_s)$, $\underline{\widetilde{f}}(t_s)$ and thresholded $\underline{\widetilde{f}}(t_s)$ with $\eta = 0.8$.

1.6 Performance indexes

Starting form the estimated $\underline{\hat{x}}$ the directions of arrival are estimated by extracting the positions of the non-zero elements of $\underline{\hat{x}}$

$$\underline{\widetilde{\theta}} = \left\{\widetilde{\theta}_l : l = 1, \dots, \widetilde{L}\right\} = \{\theta_k : |f_k| \neq 0, k = 1, \dots, K\}.$$

1.6.1 Definiton of Root Mean Square Errors $RMSE_\theta$

In order to compute the error on the estimated DoAs by taking also into account of the error on the estimation of the signal number, the $RMSE$ (averaged over Q different estimations) is defined as

$$RMSE = \frac{1}{Q}\sum_{q=1}^{Q} RMSE^{(q)} \tag{16}$$

where

$$RMSE^{(q)} = \begin{cases} \sqrt{\frac{1}{L}\left\{\sum_{l=1}^{\widetilde{L}^{(q)}} \left|\theta_l - \widetilde{\theta}_l^{(q)}\right|^2 + \left|L - \widetilde{L}^{(q)}\right| \max\left(\Delta\theta\right)^2\right\}} & if\ \widetilde{L}^{(q)} \leq L \\ \sqrt{\frac{1}{L}\left\{\sum_{l=1}^{L} \left|\theta_l - \widetilde{\theta}_l^{(q)}\right|^2 + \sum_{l=L+1}^{\widetilde{L}} \left|\widetilde{\theta}_l^{(q)} - \hat{\theta}_l^{(q)}\right|^2\right\}} & if\ \widetilde{L}^{(q)} > L \end{cases} \tag{17}$$

where $\max\left(\Delta\theta\right)^2$ is a maximum error (e.g. $\max\left(\Delta\theta\right) = 180\,[deg]$) and where

$$\hat{\theta}_l^{(q)} = \arg\left\{\min_{j=L+1} \left|\ \widetilde{\theta}_l^{(q)} - \theta_j\right|\right\}. \tag{18}$$

If $\widetilde{L}^{(q)} \leq L$ we the order of the sequence $\underline{\theta}$ until the term $\sum_{l=1}^{\widetilde{L}^{(q)}} \left|\theta_l - \widetilde{\theta}_l^{(q)}\right|^2$ of the summation (17) is minimized. Otherwise, if $\widetilde{L}^{(q)} > L$, we change the order of the sequence $\underline{\widetilde{\theta}}$. It is worth to point out that if $\widetilde{L} = L$ this definition of the $RMSE$ becomes equivalent to the standard definition used in literature.

1.6.2 Probability of correct detection P_L

The probability of correct detection P_L is defined as

$$P_L = \frac{1}{Q}\sum_{q=1}^{Q} P_L^{(q)}, \tag{19}$$

where $P_L^{(q)}$ is defined as

$$P_L^{(q)} = \begin{cases} 1 & if\, \widetilde{L}^{(q)} = L \\ 0 & otherwise \end{cases}, \; q = 1, \ldots, Q. \tag{20}$$

2 Calibration of the BCS Solver

2.1 Calibration of parameters σ_0^2 and η

GOAL: The goal of this section is to find the σ_0^2 and η values that maximize the detection probability P_L.

- Scenario parameters
  - $BPSK$ signals ($E_l^{inc} \in \{-1, 1\}$).
  - Number of signals: $L \in [2, 6]$.
  - Acutal DoAs
    - $\underline{\theta} = \underline{\theta}^{(q)}$ (the DoAs changes randomly among the different realizations).
    - $\theta_l \in [-90, 90]\,[deg]$.
  - Minimum distance among incident signals: $\Delta\theta_{min}^{l(l+1)} = 1\,[deg]$.
  - Signal to noise ratio of measured data $\underline{\nu}$: $SNR^{Eledia} = \{2, 5, 10, 20\}\,[dB]$.
- Array parameters
  - Number of array elements: $M = 20$.
  - Spacing between array elements: $d = 0.5\lambda$.
- BCS parameters
  - Initial estimate of the error term: $\sigma_0^2 \in \left[10^{-6}, 1.0\right]$.
  - Number of possible DoAs: $K = 181$.
- Simulation parameters
  - Number of realizations: $Q = 250$ (250 independent runs).
- Energy threshold values $\eta \in [0, 1]$.

2.1.1 Analysis of $P_L\left(\sigma_0^2, \eta | L, SNR\right)$ and $RMSE\left(\sigma_0^2, \eta | L, SNR\right)$

Analysis for $L = 2$ impinging signals and $SNR \in \{2, 5, 10, 20\}$

SNR $[dB]$	$\max\{P_L\}$	$\sigma_0^2 \| P_L = \max\{P_L\}$	$\eta \| P_L = \max\{P_L\}$	$\min\{RMSE\}$	$\sigma_0^2 \| RMSE = \min\{RMSE\}$	$\eta \| RMSE = \min\{RMSE\}$
2	0.804	1.00	0.85	19.781	1.0	0.90
5	0.884	10^{-1}	0.70	13.374	4.642×10^{-1}	0.90
10	0.940	2.154×10^{-1}	0.85	6.770	2.154×10^{-1}	0.95
20	0.960	4.642×10^{-2}	0.85	7.256	2.154×10^{-2}	0.90

Table 1: Table reporting the best P_L and $RMSE$ values and the corresponding locations $\left(\sigma_0^2, \eta\right)$.

$SNR = 2\ dB$ $SNR = 5\ dB$

P_L

$RMSE$

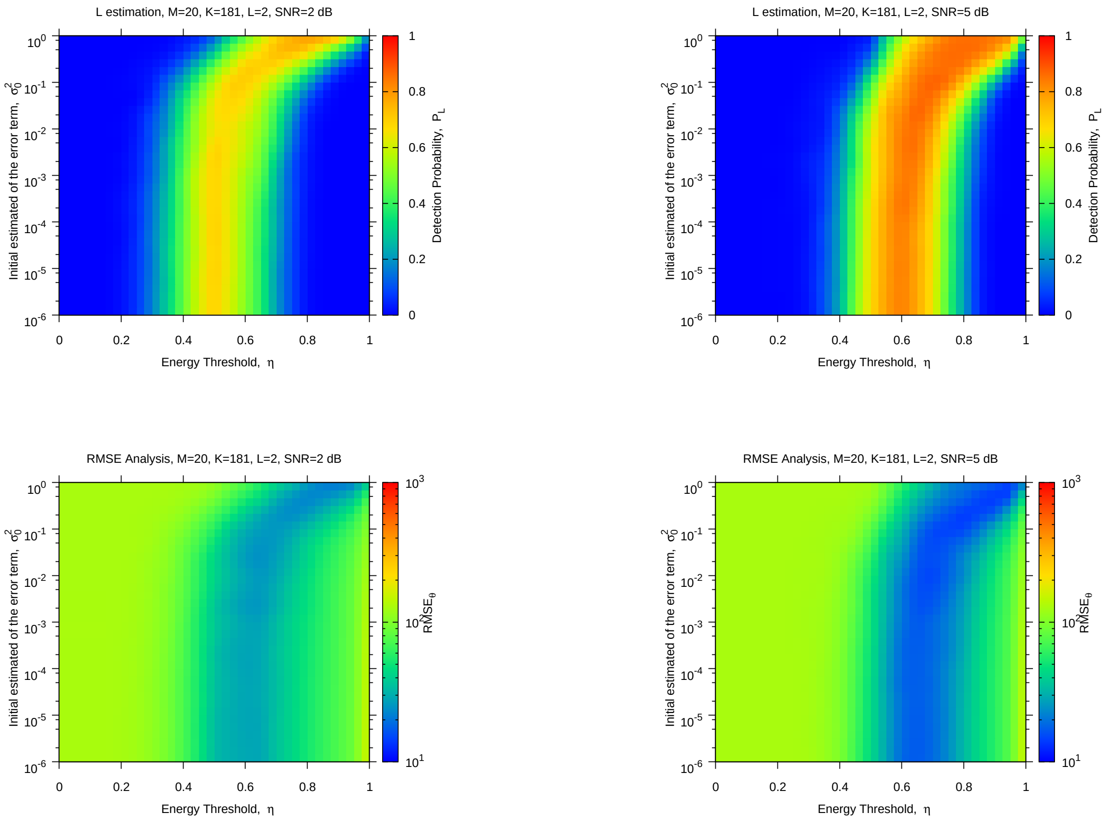

Figure 5: *BCS DoA estimation* - Detection probability P_L and $RMSE$ vs the energy threshold η and σ_0^2 when $L = 2$ signals impinges on the antenna with $SNR = 2\ dB$ and $SNR = 5\ dB$.

$SNR = 10\ dB$ $SNR = 20\ dB$

P_L

$RMSE$

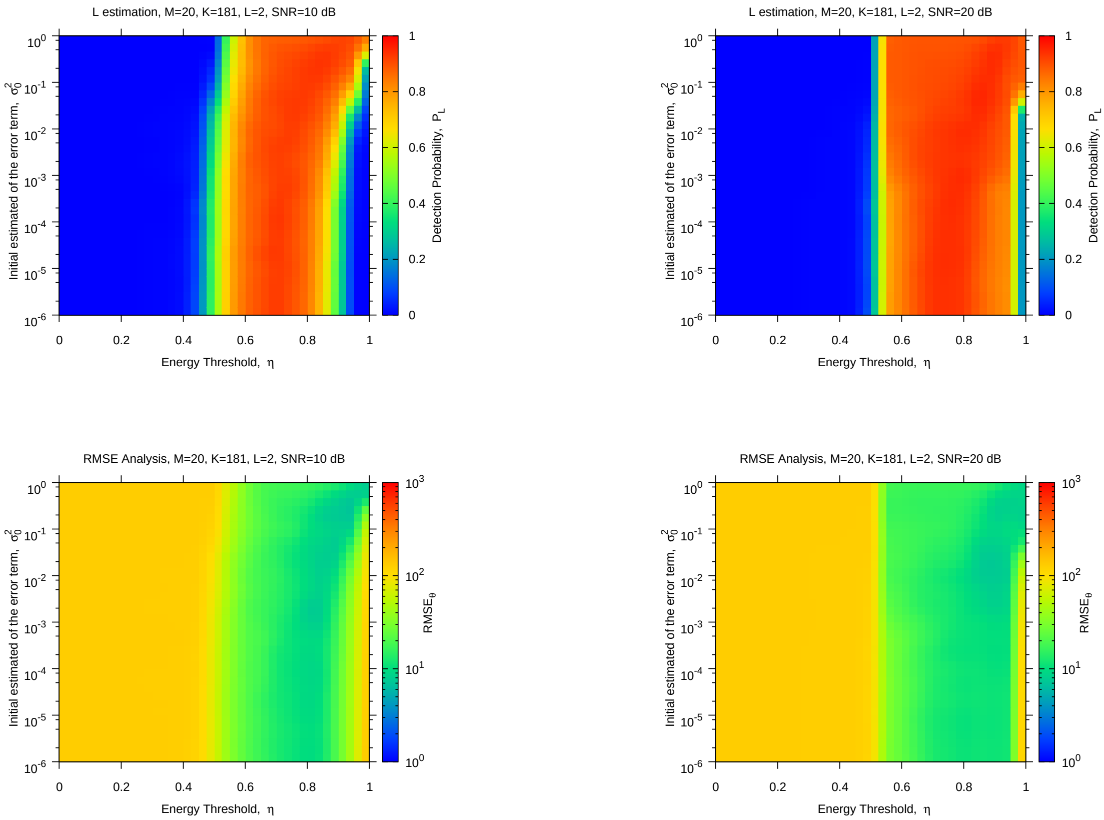

Figure 6: *BCS DoA estimation* - Detection probability P_L and $RMSE$ vs the energy threshold η and σ_0^2 when $L = 2$ signals impinges on the antenna with $SNR = 10\ dB$ and $SNR = 20\ dB$.

Analysis for $L = 4$ impinging signals and $SNR \in \{2, 5, 10, 20\}$

SNR $[dB]$	$\max\{P_L\}$	$\sigma_0^2 \mid P_L = \max\{P_L\}$	$\eta \mid P_L = \max\{P_L\}$	$\min\{RMSE\}$	$\sigma_0^2 \mid RMSE = \min\{RMSE\}$	$\eta \mid RMSE = \min\{RMSE\}$
2	0.416	10^{-3}	0.65	24.846	1.00	1.00
5	0.480	4.642×10^{-1}	0.90	23.806	4.642×10^{-2}	0.90
10	0.612	2.154×10^{-1}	0.95	19.404	10^{-2}	0.95
20	0.736	4.642×10^{-2}	0.95	13.413	10^{-1}	1.00

Table 2: Table reporting the best P_L and $RMSE$ values and the corresponding locations $\left(\sigma_0^2, \eta\right)$.

$SNR = 2\ dB$ $SNR = 5\ dB$

P_L

$RMSE$

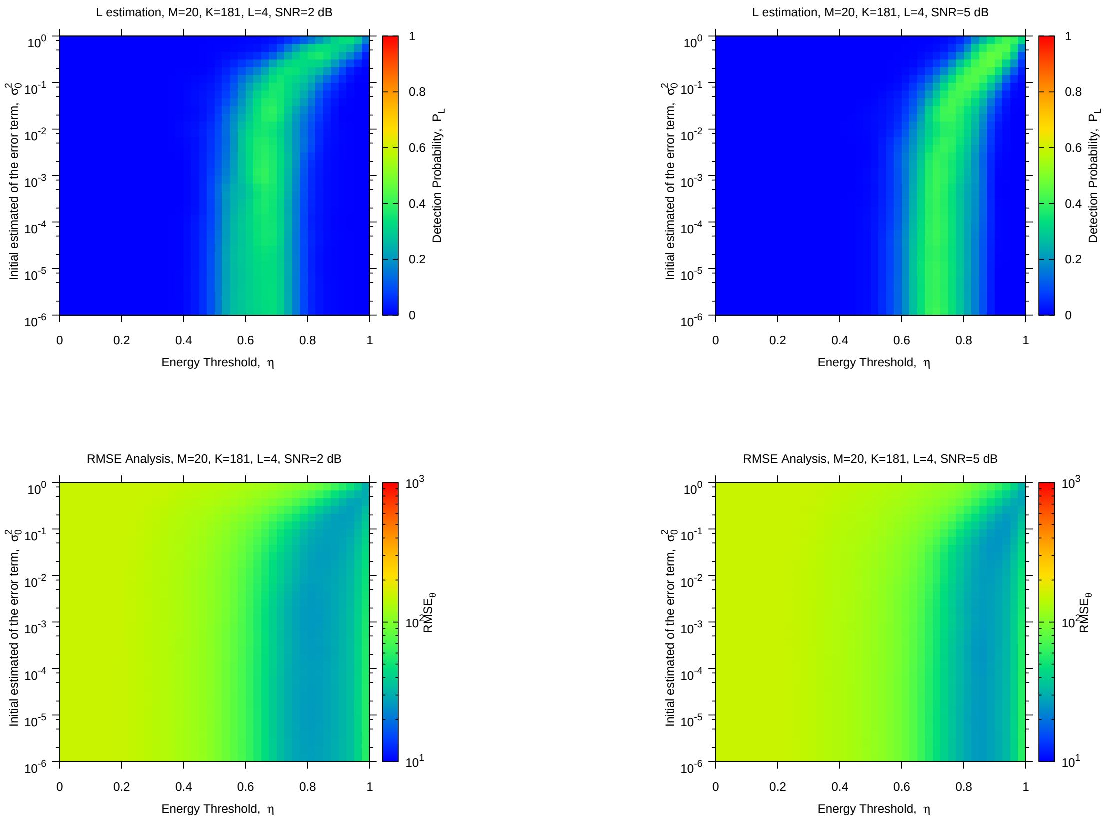

Figure 7: *BCS DoA estimation* - Detection probability P_L and $RMSE$ vs the energy threshold η and σ_0^2 when $L = 2$ signals impinges on the antenna with $SNR = 2\ dB$ and $SNR = 5\ dB$.

$SNR = 10\ dB$ $SNR = 20\ dB$

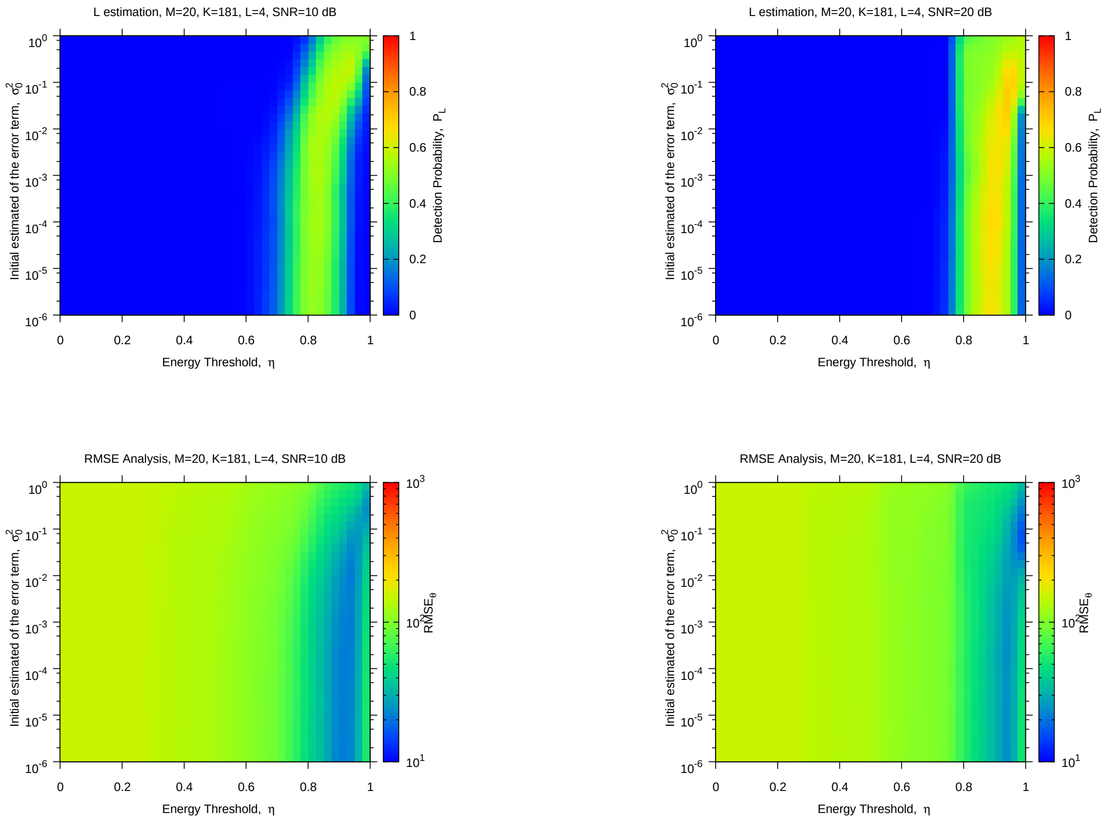

P_L

$RMSE_\theta$

Figure 8: *BCS DoA estimation* - Detection probability P_L and $RMSE$ vs the energy threshold η and σ_0^2 when $L = 2$ signals impinges on the antenna with $SNR = 10\ dB$ and $SNR = 20\ dB$.

Analysis for $L = 6$ impinging signal

SNR $[dB]$	$\max\{P_L\}$	$\sigma_0^2 \vert P_L = \max\{P_L\}$	$\eta \vert P_L = \max\{P_L\}$	$\min\{RMSE\}$	$\sigma_0^2 \vert RMSE = \min\{RMSE\}$	$\eta \vert RMSE = \min\{RMSE\}$
2	32.400	2.154×10^{-3}	0.75	22.314	4.642×10^{-2}	0.95
5	32.000	$1.0E-2$	0.85	19.870	10^{-2}	0.95
10	34.000	4.642×10^{-3}	0.90	18.294	4.642×10^{-4}	0.95
20	43.600	2.154×10^{-3}	0.95	15.251	4.642×10^{-2}	1.00

Table 3: Table reporting the best P_L and $RMSE$ values and the corresponding locations (σ_0^2, η).

$SNR = 2\ dB$ $SNR = 5\ dB$

P_L

$RMSE$

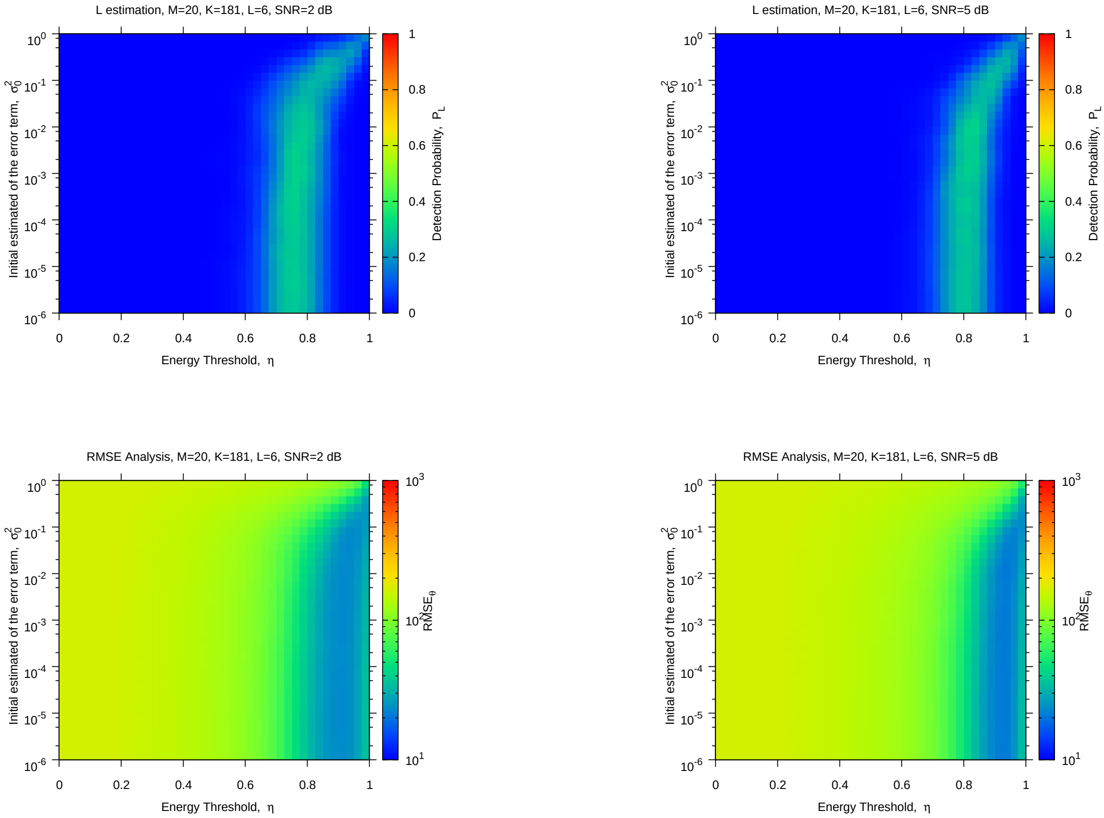

Figure 9: *BCS DoA estimation* - Detection probability P_L and $RMSE$ vs the energy threshold η and σ_0^2 when $L = 2$ signals impinges on the antenna with $SNR = 2\ dB$ and $SNR = 5\ dB$.

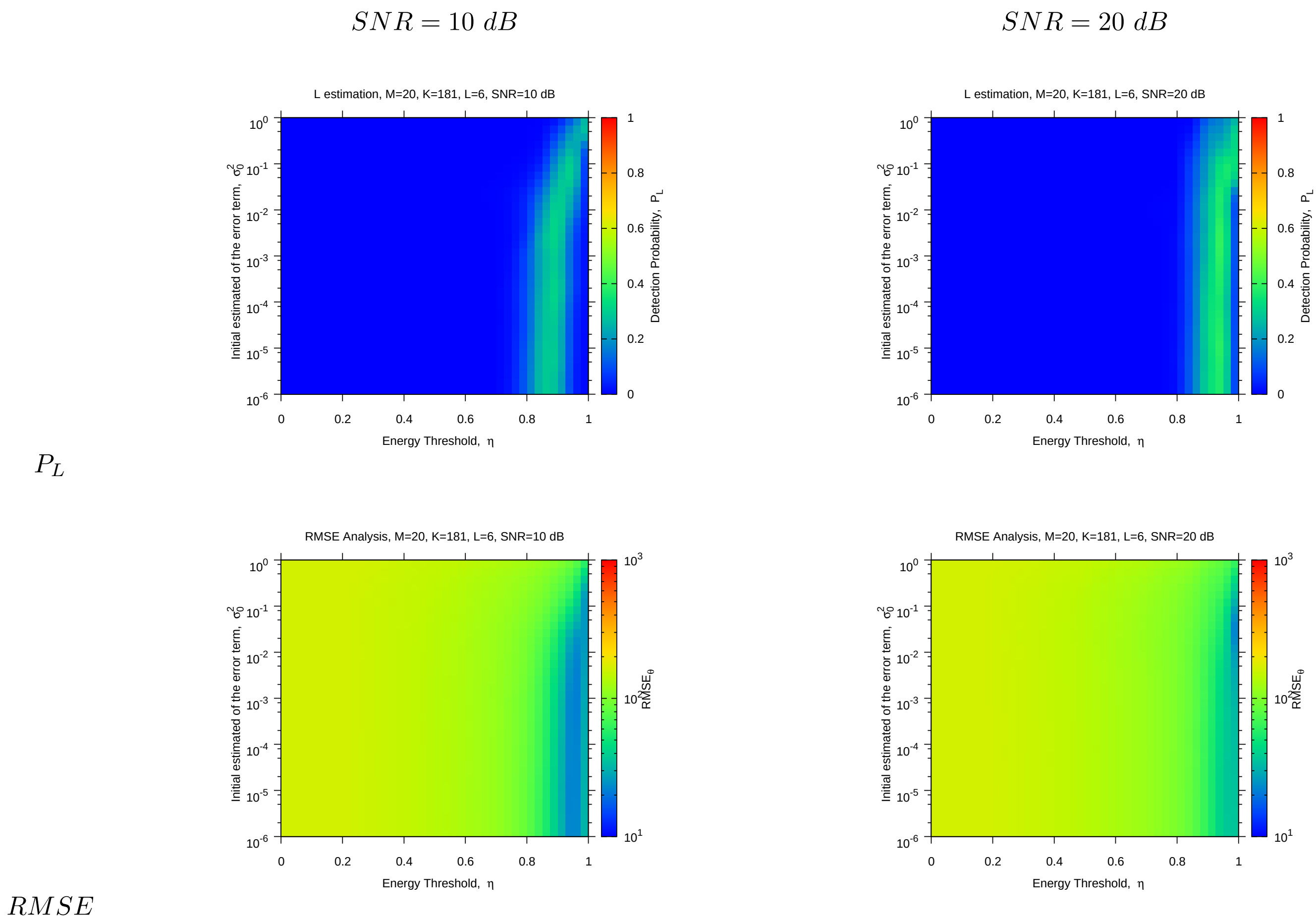

Figure 10: *BCS DoA estimation* - Detection probability P_L and $RMSE$ vs the energy threshold η and σ_0^2 when $L = 2$ signals impinges on the antenna with $SNR = 10\ dB$ and $SNR = 20\ dB$.

2.1.2 Averaged map for the identification of $\left(\sigma_0^2, \eta\right)^{opt}$ wrt P_L

The optimal σ_0^2 and η values are computed as

$$\left(\sigma_0^2, \eta\right)^{(opt)} = \arg\left\{\max_{\left(\sigma_0^2, \eta\right)} \left\{\overline{P_L}\left(\sigma_0^2, \eta\right)\right\}\right\} \tag{21}$$

where

$$\overline{P_L}\left(\sigma_0^2, \eta\right) = \sum_{SNR \in \{2,5,10,20\}} \sum_{L \in \{2,4,6\}} \frac{P_L\left(\sigma_0^2, \eta | SNR, L\right)}{\max_{\left(\sigma_0^2, \eta\right)} \left\{P_L\left(\sigma_0^2, \eta | SNR, L\right)\right\}}. \tag{22}$$

Figure (11) shows the normalized $\overline{P_L}\left(\sigma_0^2, \eta\right)$ value

$$\overline{P_L}^{norm}\left(\sigma_0^2, \eta\right) = \frac{\overline{P_L}\left(\sigma_0^2, \eta\right)}{\max_{\left(\sigma_0^2, \eta\right)} \left\{\overline{P_L}\left(\sigma_0^2, \eta\right)\right\}}. \tag{23}$$

As it can be observed, the maximum of P_L is located in $\left(\sigma_0^2, \eta\right)^{(opt)} = \left(4.642 \times 10^{-1}, 0.95\right)$: this values will be used for the next performance analysis of the method.

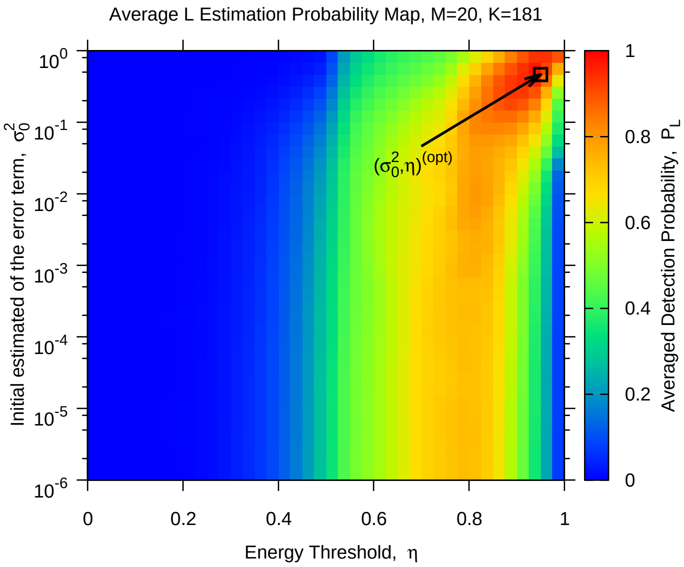

Figure 11: *Averaged detection probability map* - $\overline{P_L}^{norm}$ vs σ_0^2 and η. $\left(\sigma_0^2, \eta\right)^{(opt)} = \left(4.642 \times 10^{-1}, 0.95\right)$.

	$L = 2$		$L = 4$		$L = 6$	
SNR $[dB]$	$P_L\left(\sigma_0^2,\eta\right)^{(opt)}$	$RMSE_\theta\left(\sigma_0^2,\eta\right)^{(opt)}$ $[deg]$	$P_L\left(\sigma_0^2,\eta\right)^{(opt)}$	$RMSE_\theta\left(\sigma_0^2,\eta\right)^{(opt)}$ $[deg]$	$P_L\left(\sigma_0^2,\eta\right)^{(opt)}$	$RMSE_\theta\left(\sigma_0^2,\eta\right)^{(opt)}$ $[deg]$
2	0.184	35.01	0.200	27.15	0.244	49.20
5	0.644	14.88	0.432	32.12	0.244	66.47
10	0.892	7.05	0.552	43.75	0.228	70.92
20	0.924	8.14	0.592	41.47	0.200	74.23

Table 4: P_L and $RMSE$ for the optimal values $\left(\sigma_0^2, \eta\right)^{(opt)} = \left(4.642 \times 10^{-1}, 0.95\right)$.

	$SNR = 10\ dB$
$L = 2$	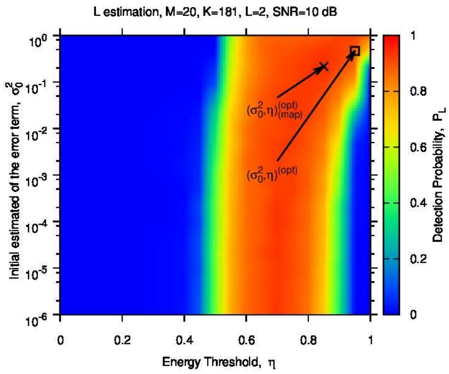
$L = 4$	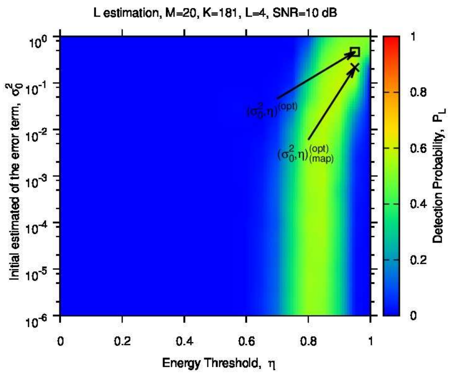
$L = 6$	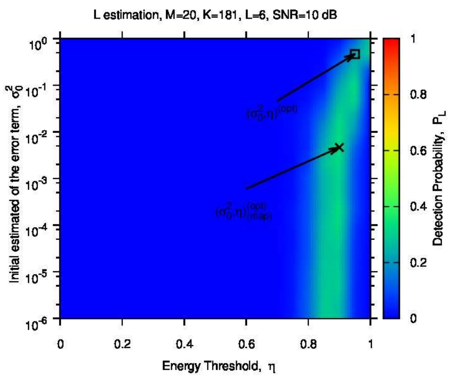

Figure 12: Location of the global $\left(\sigma_0^2, \eta\right)^{(opt)}$ global optimum value and $\left(\sigma_0^2, \eta\right)^{(opt)}_{(map)}$, the optimum of the considered map.

2.1.3 Averaged map for the identification of $\left(\sigma_0^2, \eta\right)^{opt}$ wrt $RMSE$

The optimal σ_0^2 and η values are computed as

$$\left(\sigma_0^2, \eta\right)^{(opt)} = \arg\left\{\min_{\left(\sigma_0^2, \eta\right)} \left\{\overline{RMSE}\left(\sigma_0^2, \eta\right)\right\}\right\} \tag{24}$$

where

$$\overline{RMSE}_\theta\left(\sigma_0^2, \eta\right) = \sum_{SNR \in \{2,5,10,20\}} \sum_{L \in \{2,4,6\}} RMSE\left(\sigma_0^2, \eta | SNR, L\right). \tag{25}$$

As it can be observed, the minimum of P_L is located in $\left(\sigma_0^2, \eta\right)^{(opt)} = \left(4.642 \times 10^{-1}, 1.00\right)$: this values will be used for the next performance analysis of the method.

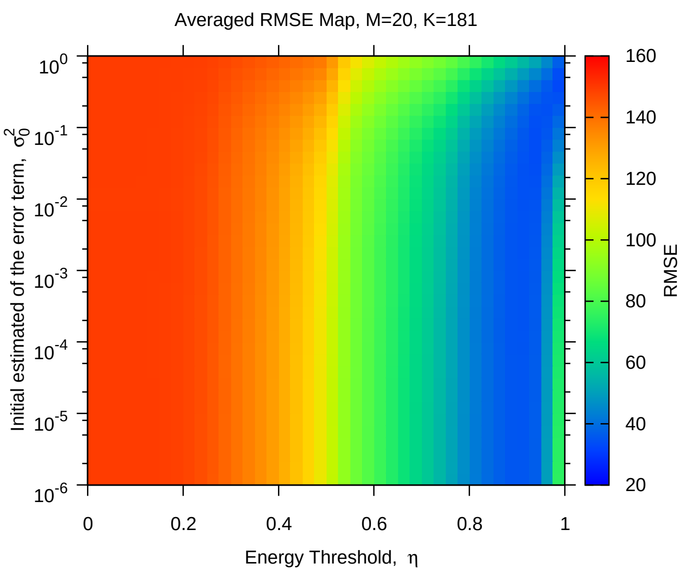

Figure 13: *Averaged detection probability map* - $\overline{RMSE}_\theta$ vs σ_0^2 and η. $\overline{RMSE}_\theta\left(\sigma_0^2, \eta\right)^{(opt)} = 29.73\,[deg]$, $\left(\sigma_0^2, \eta\right)^{(opt)} = \left(4.642 \times 10^{-1}, 1.00\right)$.

	$L=2$		$L=4$		$L=6$	
SNR $[dB]$	$P_L\left(\sigma_0^2, \eta\right)^{(opt)}$	$RMSE_\theta\left(\sigma_0^2, \eta\right)^{(opt)}$ $[deg]$	$P_L\left(\sigma_0^2, \eta\right)^{(opt)}$	$RMSE_\theta\left(\sigma_0^2, \eta\right)^{(opt)}$ $[deg]$	$P_L\left(\sigma_0^2, \eta\right)^{(opt)}$	$RMSE_\theta\left(\sigma_0^2, \eta\right)^{(opt)}$ $[deg]$
2	0.00	72.30	0.00	29.84	0.016	22.92
5	0.032	19.38	0.020	25.35	0.076	21.91
10	0.676	9.03	0.424	21.14	0.288	33.69
20	0.880	8.87	0.564	21.69	0.348	40.33

Table 5: P_L and $RMSE$ for the optimal values $\left(\sigma_0^2, \eta\right)^{(opt)} = \left(4.642 \times 10^{-1}, 0.95\right)$.

2.2 Calibration of parameters σ_0^2 and η - Noise generated starting from the definition commonly used in DoA literature

GOAL: The goal of this section is to find the σ_0^2 and η values that maximize the detection probability P_L.

- Scenario parameters
  - $BPSK$ signals ($E_l^{inc} \in \{-1, 1\}$)
  - Actual DoAs ($\theta_l^{(q)}(t_s) = \theta_l^{(q)}\ \forall s$, $l = 1, \dots, L$, $q = 1, \dots, Q$)
  - Number of signals: $L \in [2, 6]$.
  - Minimum distance among incident signals: $\Delta\theta_{min}^{l(l+1)} = 1\,[deg]$.
  - $\theta_l \in [-90, 90]\,[deg]$
  - Signal to noise ratio of measured data $\underline{\nu}(t_s)$: $SNR^{lit} = \{2, 5, 10, 20\}\,[dB]$.
- Array parameters
  - Number of array elements: $M = 20$.
  - Spacing between array elements: $d = 0.5\lambda$.
- BCS parameters
  - Initial estimate of the error term: $\sigma_0^2 \in \left[10^{-6}, 1.0\right]$
  - Number of possible DoAs: $K = 181$
  - Number of snapshots: $S = 1$
  - Number of realizations: $Q = 250$
  - Energy threshold values $\eta \in [0, 1]$

2.2.1 Analysis of $P_L\left(\sigma_0^2, \eta | L, SNR\right)$ and $RMSE\left(\sigma_0^2, \eta | L, SNR\right)$

Analysis for $L = 2$ impinging signals

SNR $[dB]$	$\max\{P_L\}$	$\sigma_0^2 \| P_L = \max\{P_L\}$	$\eta \| P_L = \max\{P_L\}$
2	0.912	4.642×10^{-1}	0.80
5	0.936	2.154×10^{-1}	0.85
10	0.948	4.642×10^{-2}	0.85
20	0.948	2.154×10^{-1}	0.85

Table 6: Table reporting the best P_L value and the corresponding location $\left(\sigma_0^2, \eta\right)$.

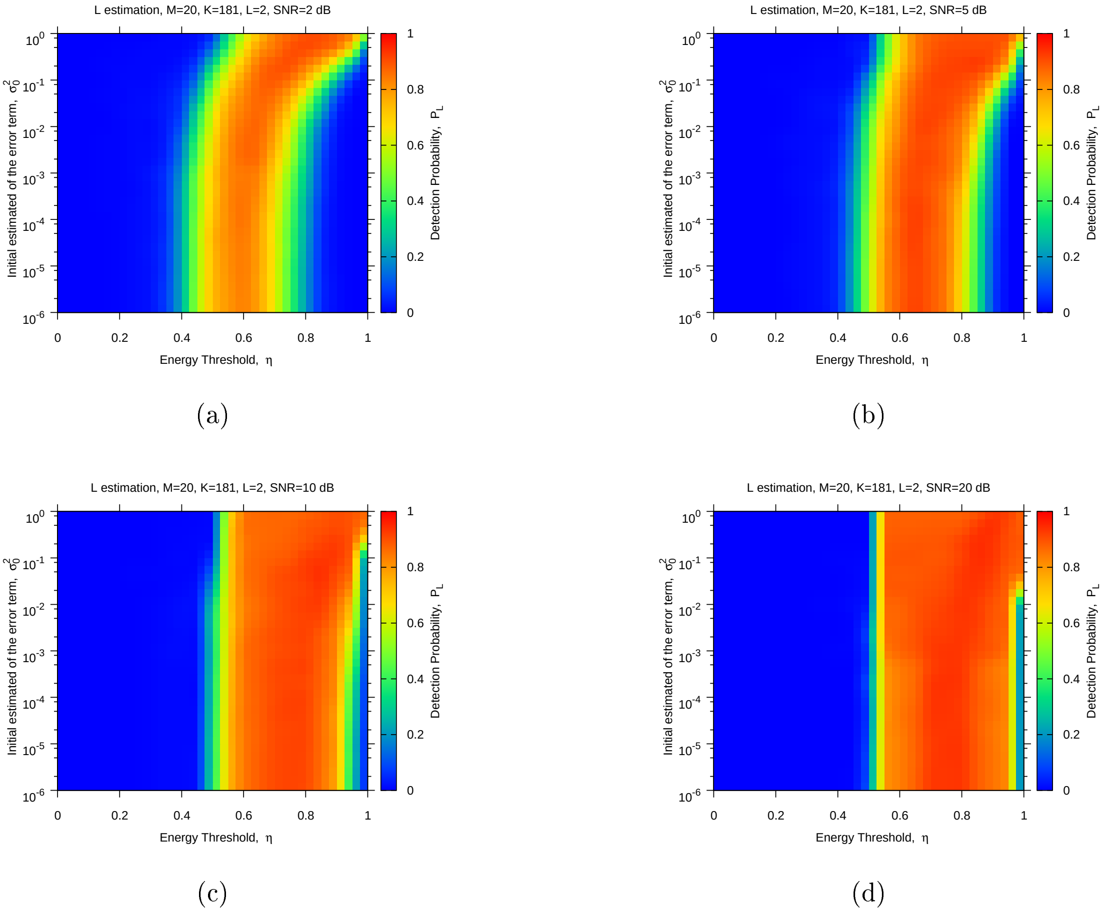

Figure 14: *BCS DoA estimation* - Detection probability P_L vs the energy threshold η and σ_0^2 when $L = 2$ signals impinges on the antenna with (a) $SNR = 2$ dB, (b) $SNR = 5$ dB, (c) $SNR = 10$ dB and , (d) $SNR = 20$ dB.

Analysis for $L = 4$ impinging signals

SNR $[dB]$	$\max\{P_L\}$	$\sigma_0^2 \vert P_L = \max\{P_L\}$	$\eta \vert P_L = \max\{P_L\}$
2	0.668	2.154×10^{-1}	0.90
5	0.668	2.154×10^{-1}	0.95
10	0.736	10^{-1}	0.95
20	0.716	2.154×10^{-2}	0.95

Table 7: Table reporting the best P_L value and the corresponding location (σ_0^2, η).

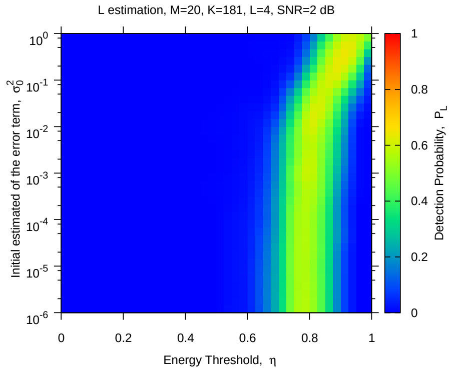

(a)

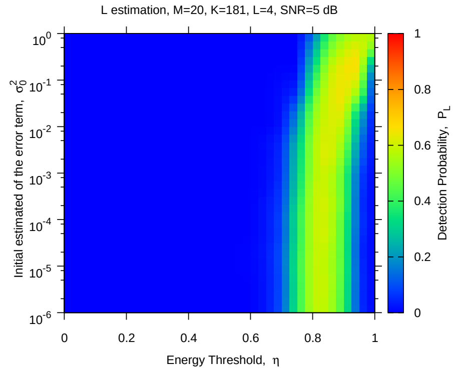

(b)

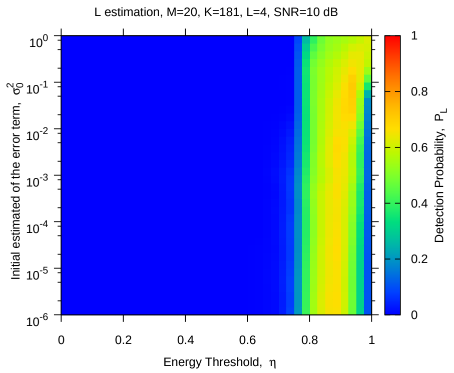

(c)

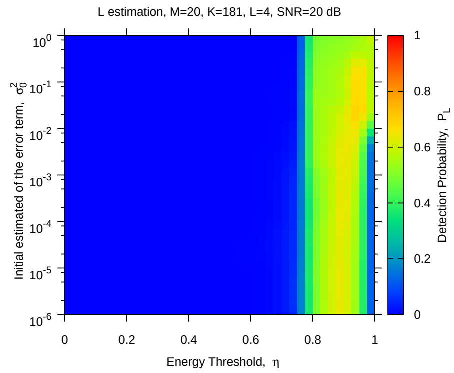

(d)

Figure 15: *BCS DoA estimation* - Detection probability P_L vs the energy threshold η and σ_0^2 when $L = 4$ signals impinges on the antenna with (a) $SNR = 2\ dB$, (b) $SNR = 5\ dB$, (c) $SNR = 10\ dB$ and , (d) $SNR = 20\ dB$.

Analysis for $L = 6$ impinging signal

$SNR\ [dB]$	$\max\{P_L\}$	$\sigma_0^2 \| P_L = \max\{P_L\}$	$\eta \| P_L = \max\{P_L\}$
2	0.344	2.154×10^{-6}	0.85
5	0.416	10^{-3}	0.90
10	0.392	2.154×10^{-2}	0.95
20	0.516	4.642×10^{-3}	0.95

Table 8: Table reporting the best P_L value and the corresponding location (σ_0^2, η).

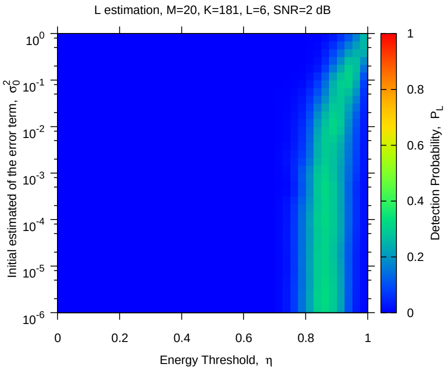

(a)

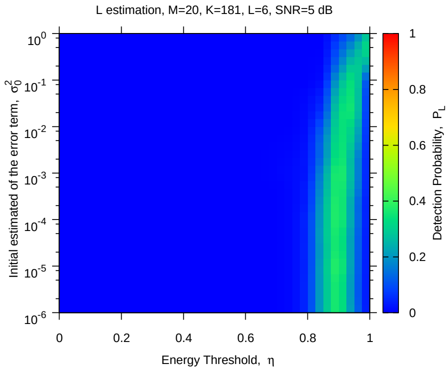

(b)

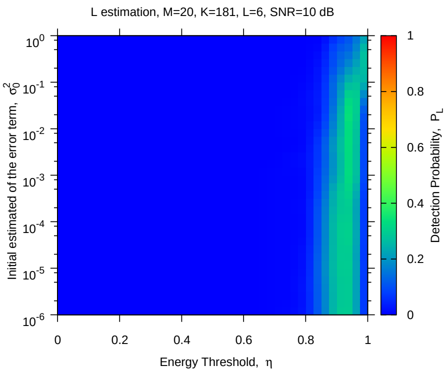

(c)

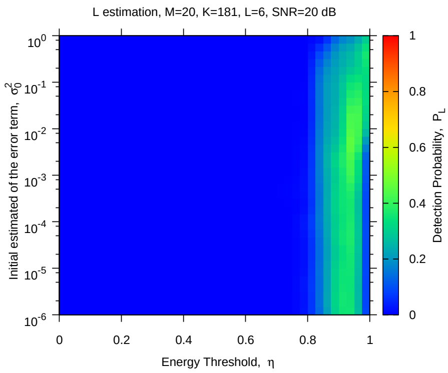

(d)

Figure 16: *BCS DoA estimation* - Detection probability P_L vs the energy threshold η and σ_0^2 when $L = 6$ signals impinges on the antenna with (a) $SNR = 2\ dB$, (b) $SNR = 5\ dB$, (c) $SNR = 10\ dB$ and , (d) $SNR = 20\ dB$.

2.2.2 Averaged map for the identification of $\left(\sigma_0^2, \eta\right)^{opt}$

As it can be observed, the maximum of P_L is located in $\left(\sigma_0^2, \eta\right)^{(opt)} = \left(2.154 \times 10^{-1}, 0.95\right)$: this values will be used for the next performance analysis of the method.

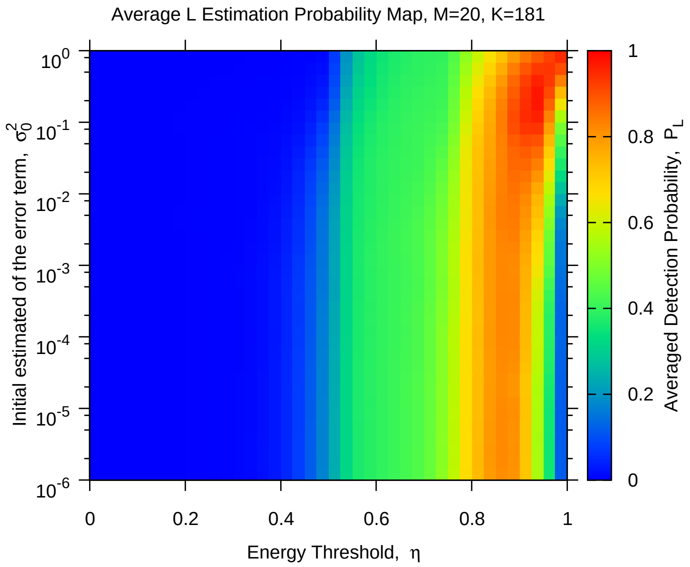

Figure 17: *Averaged detection probability map* - $\overline{P_L}^{norm}$ vs σ_0^2 and η. $\left(\sigma_0^2, \eta\right)^{(opt)} = \left(2.154 \times 10^{-1}, 0.95\right)$.

	$L = 2$		$L = 4$		$L = 6$	
SNR $[dB]$	P_L	$RMSE$ $[deg]$	P_L	$RMSE$ $[deg]$	P_L	$RMSE$ $[deg]$
2	0.224	10.67	0.540	5.60	0.336	11.66
5	0.780	5.22	0.668	5.51	0.316	9.75
10	0.896	3.27	0.668	4.81	0.208	6.51
20	0.900	3.12	0.684	6.32	0.280	4.31

Table 9: P_L and $RMSE$ for the optimal values $\left(\sigma_0^2, \eta\right)^{(opt)} = \left(2.154 \times 10^{-1}, 0.95\right)$.

More information on the topics of this document can be found in the following list of references.

References

[1] M. Carlin, P. Rocca, G. Oliveri, F. Viani, and A. Massa, "Directions-of-arrival estimation through Bayesian Compressive Sensing strategies," *IEEE Trans. Antennas Propag.*, vol. 61, no. 7, pp. 3828-3838, Jul. 2013.

[2] M. Carlin, P. Rocca, G. Oliveri, and A. Massa, "Bayesian compressive sensing as applied to directions-of-arrival estimation in planar arrays," *J. Electromagn. Waves Appl.*, vol. 2013, pp. 1-12, 2013.

[3] M. Carlin, P. Rocca, "A Bayesian compressive sensing strategy for direction-of-arrival estimation," *6th European Conference on Antennas Propag. (EuCAP 2012)*, Prague, Czech Republic, pp. 1508-1509, 26-30 Mar. 2012.

[4] A. Massa, P. Rocca, and G. Oliveri, "Compressive sensing in electromagnetics - A review," *IEEE Antennas Propag. Mag.*, pp. 224-238, vol. 57, no. 1, Feb. 2015.

[5] G. Oliveri and A. Massa, "Bayesian compressive sampling for pattern synthesis with maximally sparse non-uniform linear arrays," *IEEE Trans. Antennas Propag.*, vol. 59, no. 2, pp. 467-481, Feb. 2011.

[6] G. Oliveri, M. Carlin, and A. Massa, "Complex-weight sparse linear array synthesis by Bayesian Compressive Sampling," *IEEE Trans. Antennas Propag.*, vol. 60, no. 5, pp. 2309-2326, May 2012.

[7] G. Oliveri, P. Rocca, and A. Massa, "Reliable diagnosis of large linear arrays - A Bayesian Compressive Sensing approach," *IEEE Trans. Antennas Propag.*, vol. 60, no. 10, pp. 4627-4636, Oct. 2012.

[8] F. Viani, G. Oliveri, and A. Massa, "Compressive sensing pattern matching techniques for synthesizing planar sparse arrays," *IEEE Trans. Antennas Propag.*, vol. 61, no. 9, pp. 4577-4587, Sept. 2013.

[9] G. Oliveri, E. T. Bekele, F. Robol, and A. Massa, "Sparsening conformal arrays through a versatile BCS-based method," *IEEE Trans. Antennas Propag.*, vol. 62, no. 4, pp. 1681-1689, Apr. 2014.

[10] M. Carlin, G. Oliveri, and A. Massa, "Hybrid BCS-deterministic approach for sparse concentric ring isophoric arrays," *IEEE Trans. Antennas Propag.*, vol. 63, no. 1, pp. 378-383, Jan. 2015.

[11] L. Lizzi, F. Viani, M. Benedetti, P. Rocca, and A. Massa, "The M-DSO-ESPRIT method for maximum likelihood DoA estimation," *Prog. Electromagn. Res.*, vol. 80, pp. 477-497, 2008.

[12] M. Donelli, F. Viani, P. Rocca, and A. Massa, "An innovative multi-resolution approach for DoA estimation based on a support vector classification," *IEEE Trans. Antennas Propag.*, vol. 57, no. 8, pp. 2279-2292, Aug. 2009.

[13] L. Lizzi, G. Oliveri, P. Rocca, and A. Massa, "Estimation of the direction-of-arrival of correlated signals by means of a SVM-based multi-resolution approach," *IEEE Antennas Propag. Society International Symposium (APSURSI), Toronto, ON, Canada*, pp. 1-4, 11-17 Jul. 2010.

[14] G. Oliveri, N. Anselmi, and A. Massa, "Compressive sensing imaging of non-sparse 2D scatterers by a total-variation approach within the Born approximation," *IEEE Trans. Antennas Propag.*, vol. 62, no. 10, pp. 5157-5170, Oct. 2014.

[15] L. Poli, G. Oliveri, and A. Massa, “Imaging sparse metallic cylinders through a Local Shape Function Bayesian Compressive Sensing approach,” *J. Opt. Soc. Am. A*, vol. 30, no. 6, pp. 1261-1272, 2013.

[16] F. Viani, L. Poli, G. Oliveri, F. Robol, and A. Massa, “Sparse scatterers imaging through approximated multitask compressive sensing strategies,” *Microwave Opt. Technol. Lett.*, vol. 55, no. 7, pp. 1553-1558, Jul. 2013.

[17] L. Poli, G. Oliveri, P. Rocca, and A. Massa, “Bayesian compressive sensing approaches for the reconstruction of two-dimensional sparse scatterers under TE illumination,” *IEEE Trans. Geosci. Remote Sensing*, vol. 51, no. 5, pp. 2920-2936, May 2013.

[18] L. Poli, G. Oliveri, and A. Massa, “Microwave imaging within the first-order Born approximation by means of the contrast-field Bayesian compressive sensing,” *IEEE Trans. Antennas Propag.*, vol. 60, no. 6, pp. 2865-2879, Jun. 2012.

[19] G. Oliveri, P. Rocca, and A. Massa, “A bayesian compressive sampling-based inversion for imaging sparse scatterers,” *IEEE Trans. Geosci. Remote Sensing*, vol. 49, no. 10, pp. 3993-4006, Oct. 2011.

[20] G. Oliveri, L. Poli, P. Rocca, and A. Massa, “Bayesian compressive optical imaging within the Rytov approximation,” *Optics Letters*, vol. 37, no. 10, pp. 1760-1762, 2012.

[21] L. Poli, G. Oliveri, F. Viani, and A. Massa, “MT-BCS-based microwave imaging approach through minimum-norm current expansion,” *IEEE Trans. Antennas Propag.*, vol. 61, no. 9, pp. 4722-4732, Sep. 2013.